Hindawi
Journal of Nanomaterials
Volume 2019, Article ID 3525143, 6 pages
https://doi.org/10.1155/2019/3525143

Research Article

Fabrication of Mn^{2+}-Doped Hollow Mesoporous Aluminosilica Nanoparticles for Magnetic Resonance Imaging and Drug Delivery for Therapy of Colorectal Cancer

Yue Lu,[1,2] Shirui Zhao,[1] and Xin-an Zhang[1]

[1]*School of Kinesiology, Shenyang Sport University, Shenyang, 110102 Liaoning, China*
[2]*Anorectal Ward III, The Third Affiliated Hospital of Liaoning University of Traditional Chinese Medicine, Shenyang, 110003 Liaoning, China*

Correspondence should be addressed to Xin-an Zhang; zhangxa2725@163.com

Received 17 July 2019; Accepted 6 September 2019; Published 3 November 2019

Academic Editor: Ruibing Wang

A novel Mn^{2+}-doped hollow Mn-HMAS aluminosilica (Mn-HMAS) nanoparticle for simultaneous T_1-weighted magnetic resonance imaging and drug delivery was reported. The magnetic resonance tests showed that the Mn-HMAS nanoparticles display an excellent T_1-weighted magnetic resonance imaging effect with a high T_1 relaxivity (r1) of 8.8 $mM^{-1}S^{-1}$. The MTT assays showed that the Mn-HMAS-DOX nanoparticles possess a better tumour cell inhibition effect than DOX. In addition, the Mn-HMAS nanoparticles also exhibit good stability and noncytotoxicity. These results demonstrated that the Mn-HMAS nanoparticles can be applied for the loading and delivery of various drugs in medicine.

1. Introduction

Colorectal cancer (CRC) is the third most common malignancy worldwide in both men and women [1, 2]. It is expected that the CRC burden will increase dramatically in the next 20 years due to the popularity of Western lifestyles [3]. Currently, therapy for CRC includes surgical resection, radiation, and chemotherapy with cytocidal chemicals and biologic agents. Some targeted drugs, such as cetuximab and panimab, are used for the treatment of colorectal cancer; however, these drugs still exhibit many deleterious side effects, such as destroying DNA or inhibiting its synthesis [4, 5]. In addition, chemotherapy and biologics cause inflammatory reactions or interfere with certain aspects of it [6]. Moreover, the imprecise release and distribution of drugs in the body also affect the effectiveness of chemotherapy. Therefore, the development of new materials to enhance drug-targeting therapy is of urgency.

Hollow porous silica-based nanomaterials have attracted a great deal of interest as delivery carriers for anticancer drugs, proteins, and DNA, due to their large surface area, tuneable pore size, high drug-loading capacity, and nontoxicity [7–15]. Therefore, developing new hollow porous silica-based nanosystems for the controlled-release delivery of drugs is vital.

In recent years, multifunctional nanostructured materials have been applied to cancer diagnosis and therapy [15–23]. The dominant advantage of these multifunctional nanomaterials is that they can integrate early cancer diagnosis, targeted drug delivery, and treatment with in vivo tracing and thus improve the anticancer therapeutic efficiency. However, the synthesis of multifunctional nanosystems for simultaneous cancer diagnosis and therapy remains a challenge. Herein, we successfully synthesized Mn^{2+}-doped hollow mesoporous aluminosilica (designated as Mn-HMAS) nanoparticles by combining the in situ sacrificial template method and the ion exchange method. We also demonstrated that the Mn-HMAS nanoparticles could be used for simultaneous magnetic resonance imaging and drug delivery. In the present study, we determined that Mn-HMAS nanoparticles exhibited low cytotoxicity towards human colorectal cancer cells (HCT116 cells) and that Mn-HMAS-DOX

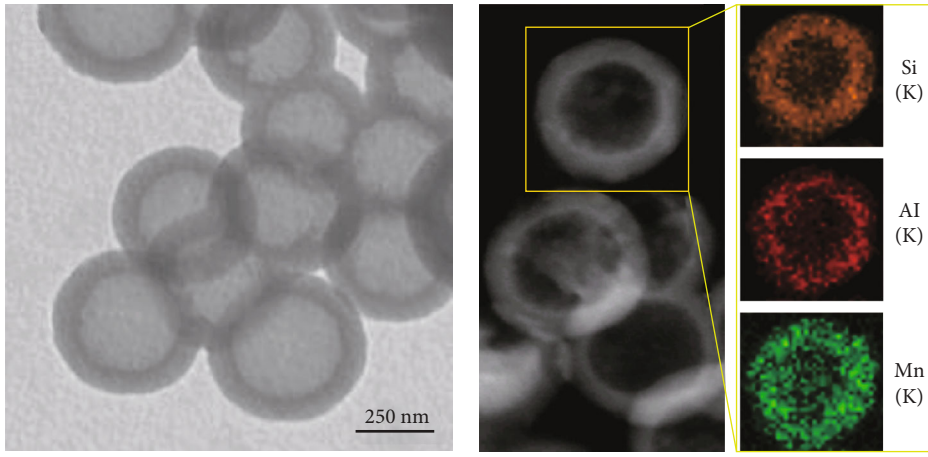

Figure 1: (a) Transmission electron microscopy (TEM) image of the Mn-HMAS nanoparticles and (b) scanning transmission electron microscopy (STEM) image and the corresponding energy-dispersive X-ray (EDS) elemental mapping images of the Mn-HMAS nanoparticles.

nanoparticles exhibited a stronger inhibition efficiency than DOX.

2. Materials and Methods

2.1. Materials. Tetraethoxysilane (TEOS) and cetyltrimethylammonium bromide (CTAB) were purchased from Alfa Aesar. $AgNO_3$, DOX, Na_2CO_3, NH_3-H_2O (ammonium aqueous solution, 25-28%), and $NaAlO_2$ were purchased from Sinopharm Chemical Reagent Co., Ltd. (Shanghai, China).

2.2. Synthesis of [Na^+]-HMAS Nanoparticles. The process of the preparation of [Na^+]-HMAS nanoparticles can be divided into the following three steps [24, 25]: (1) The *s*SiO_2 nanoparticles were synthesized through the Stöber method. Typically, 74 mL of ethanol and 3.15 mL of ammonia aqueous solution (~28%) were mixed with 10 mL of water. Then, 6 mL of TEOS was added into the mixture while being heated to 50°C and allowed to react for 6 hours. Hence, the *s*SiO_2 nanoparticles were obtained. (2) First, 50 mg of *s*SiO_2 nanoparticles was dispersed in the 10 mL aqueous solution that contained 12.5 mg of CTAB. Then, 35 mg of $NaAlO_2$ and 40 mg of Na_2CO_3 were added into the solution. The mixture was heated to 95°C and allowed to react for 4 hours. The final [Na^+]-HMAS/CTAB nanoparticles were collected by centrifugation. (3) The [Na^+]-HMAS/CTAB nanoparticles were heated to 550°C for 6 hours while continuously under atmospheric pressure to remove the remaining surfactant (CTAB) molecules.

2.3. Synthesis of Mn-HMAS Nanoparticles. First, 30 mg of [Na^+]-HMAS nanoparticles was dispersed in 6.0 mL of a 0.05 M $MnCl_2$ aqueous solution, which was continuously stirred for 24 hours at room temperature. The final product (Mn-HMAS) was collected through centrifugation and washed with distilled water.

2.4. DOX Loading and Release Tests. First, 10 mg of Mn-HMAS nanoparticles was suspended in the DOX solution (2.0 mL, 2.5 mg/mL). The mixture solution was kept for 12 hours, allowing the loading of DOX into the Mn-HMAS structure. The obtained DOX-loaded Mn-HMAS (Mn-HMAS-DOX) nanoparticles were collected by centrifugation and washed with ultrapure water. To test the release kinetics of DOX from the Mn-HMAS-DOX nanoparticles, the samples were dispersed in 1.0 mL of PBS (pH 5.0, 6.0, and 7.4) at 37°C with gentle shaking. At each time point, the solution was collected by centrifuging and replaced with fresh PBS. The amount of released DOX was tested by a UV-Vis spectrophotometry with the absorbance at 479 nm.

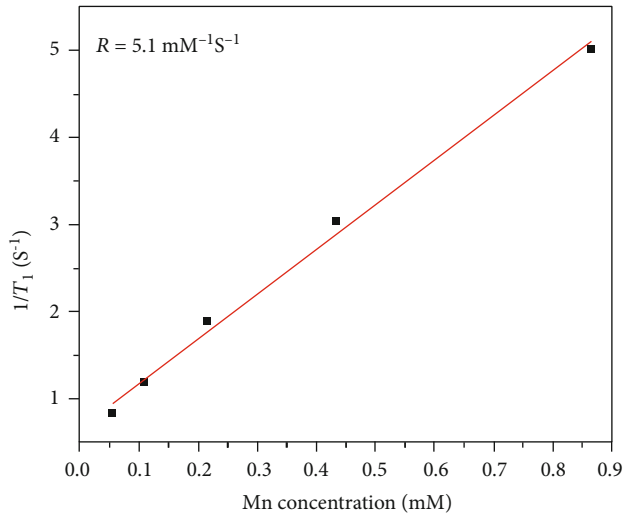

Figure 2: Plots of T_1 versus manganese ion concentrations of Mn-HMAS nanoparticles.

2.5. MRI Tests. The T_1-weighted MR images of Mn-HMAS nanoparticles were acquired on a 0.5 T NMR120-Analyst NMR system (Niumag Corporation, Shanghai, China). For the MRI test, various Mn^{2+} concentrations of nanoparticles

(a) (b)

Figure 3: T_1-weighted MR images of human colorectal cancer cells (HCT116 cells) (a) and those that were treated with Mn-HMAS nanoparticles at a concentration of 25 ppm (b).

in an aqueous solution containing 1% agar were prepared, including 0.8656, 0.4328, 0.2164, 0.1082, and 0.0541 mM. The T_1-weighted fast-recovery spin-echo (FR-FSE) sequence was as follows: TR/TE = 800/12 ms, 128 × 256 matrices, and repetition times = 4.

To evaluate the contrast effect of these nanoparticles inside the cells, HCT116 cells were seeded in 6-well plates and treated with Mn-HMAS nanoparticles (25 ppm). Six hours after the treatment, the cells were washed twice with 1 mL PBS. Then, 1 mL trypsin was added to digest the cells for 3 min, and the trypsin was discarded. The supernatant was discarded at the end of centrifugation, while the cells were resuspended with 200 μL PBS and then added into a 0.2 mL EP tube for the MRI test.

2.6. Cell Proliferation Assay. HCT116 cells were seeded into 24-well plates at a concentration of 5×10^4 cells per well. After the overnight culture, the Mn-HMAS nanoparticles were added in different concentrations. After 24 hours, cell proliferation was determined by adding the MTT solution (50 g/well) and incubating for 1 hour and then mixed with dimethyl sulfoxide after the supernatant was removed. The OD value at 570 nm was read using the microplate reader. This assay was repeated three times.

2.7. Statistical Analysis. Results were presented as the mean ± standard deviation (SD). Statistical significance was performed via one-way Student's t-test. $P < 0.05$ was considered statistically significant.

3. Results and Discussion

Hollow mesoporous aluminosilica (HMAS) nanoparticles were first synthesized using an in situ sacrificial template route reported by Liu et al. and Cabral et al. [20, 21]. Then, the Mn-HMAS nanoparticles were obtained through an ion exchange process. As shown in Figure 1(a), the Mn-HMAS nanoparticles possessed a typical hollow porous structure with an average diameter of ~450 nm and an approximately 70 nm thick shell. Energy-dispersive X-ray (EDS) spectroscopy was used to investigate the elemental distributions in the Mn-HMAS nanoparticles (Figure 1(b)). As seen, the Si, Al, and Mn elements were uniformly distributed in the Mn-HMAS nanoparticles, meaning that manganese ions were successfully loaded inside the porous structure by our ion exchange method. In addition, size distribution and zeta potential of the [Mn]-HMAS nanoparticles were

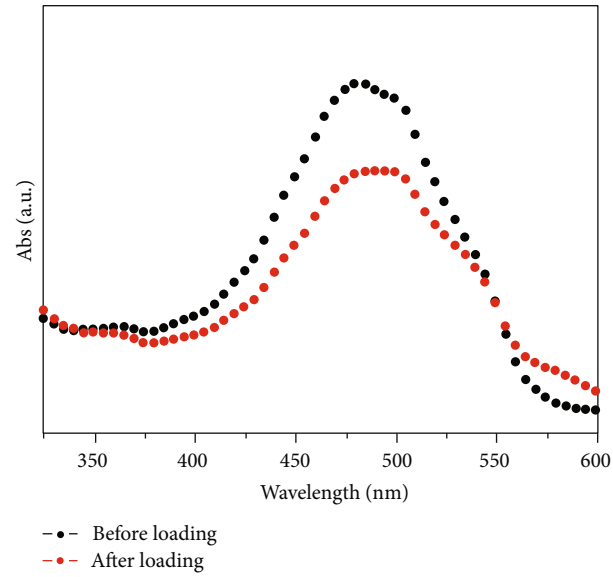

Figure 4: Absorption spectra of the solutions of DOX before and after treatment with Mn-HMAS nanoparticles.

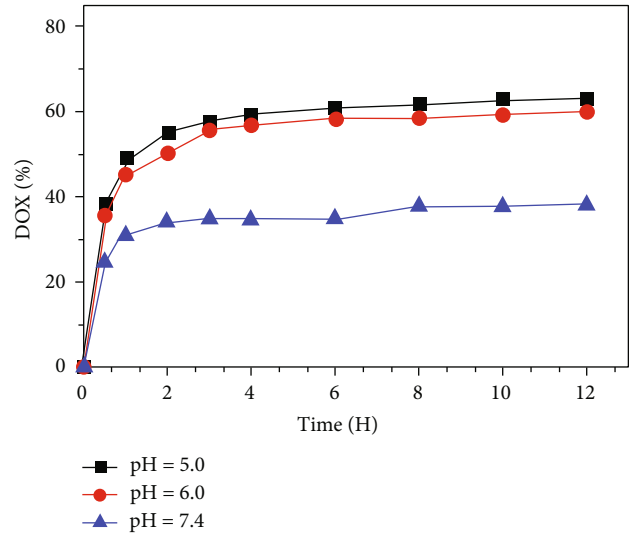

Figure 5: The DOX release from Mn-HMAS-DOX nanoparticles in PBS at varied pH values.

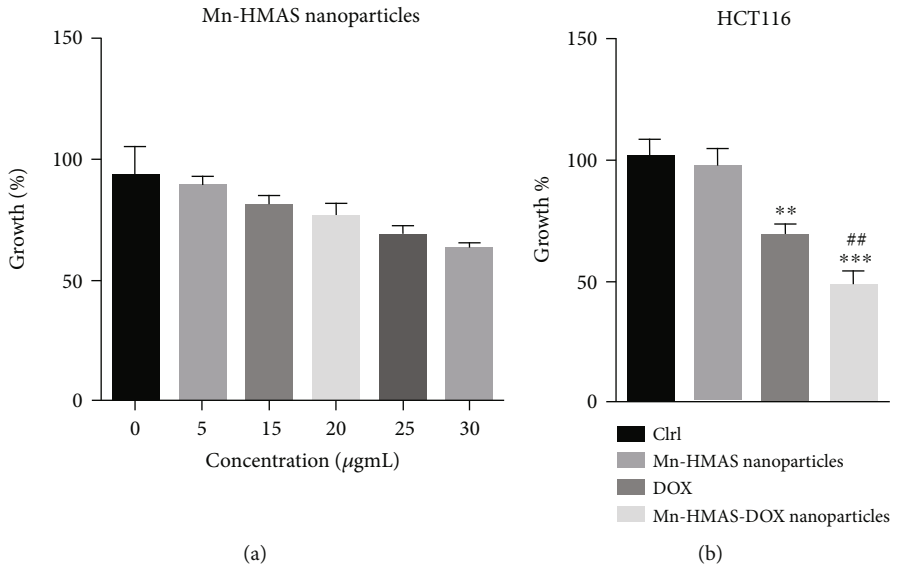

Figure 6: (a) The MTT assay checking the viability effect of Mn-HMAS nanoparticles on HCT116 cells in the absence and in the presence of various concentrations of Mn-HMAS nanoparticles for 24 hours. (b) Cell viabilities of HCT116 cells treated with Mn-HMAS nanoparticles, DOX, and Mn-HMAS-DOX nanoparticles at a Mn-HMAS nanoparticle concentration of 20 μg/mL. $^{**}P < 0.01$ and $^{***}P < 0.001$ versus no Mn-HMAS nanoparticles. $^{\#\#}P < 0.01$ versus DOX.

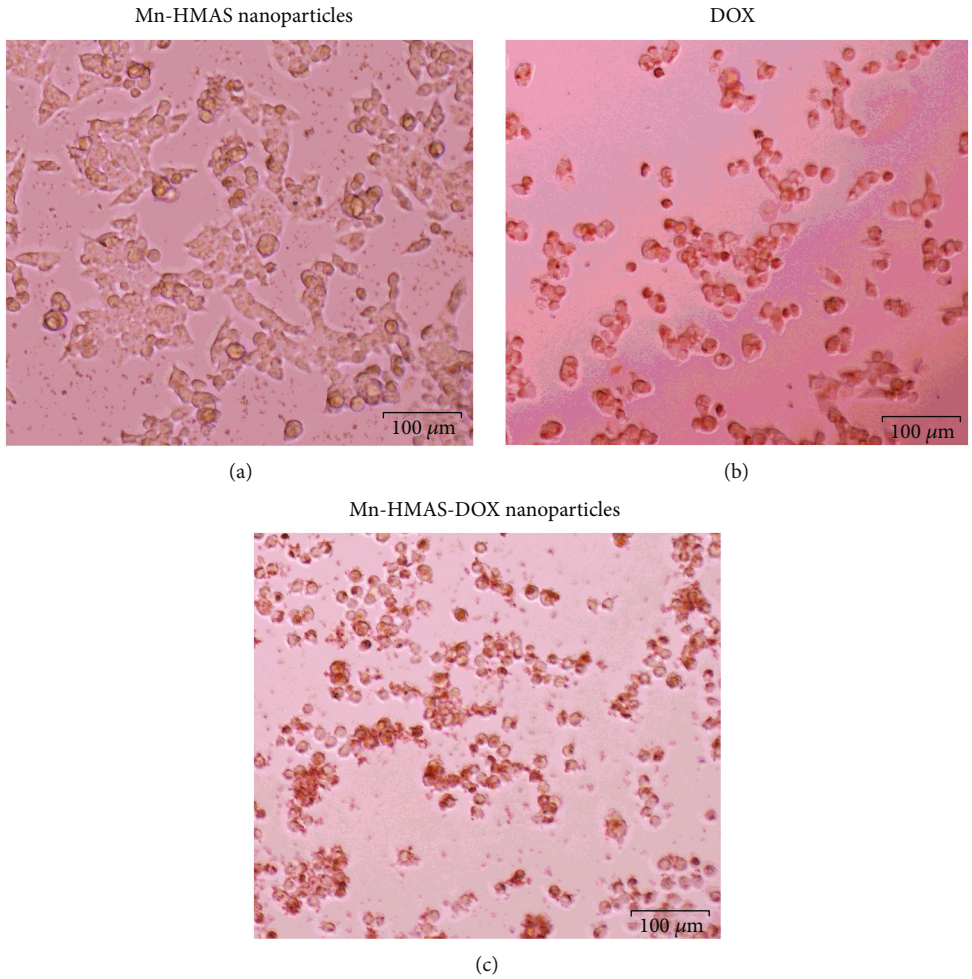

Figure 7: Light microscopic images of HCT116 cells after being treated with Mn-HMAS nanoparticles (a), DOX (b), and Mn-HMAS-DOX nanoparticles (c) for 24 hours (scale bar = 100 μm).

further determined by using dynamic light scattering (DLS) (see Figures S1 and S2).

The potential of Mn-HMAS nanoparticles as the contrast agents was tested by using a 0.5 T MRI scanner. Figure 2 shows that the T_1 relaxivity of Mn-HMAS nanoparticles was calculated as 8.8 $mM^{-1}S^{-1}$. To evaluate the contrast effect of these nanoparticles inside cells, human colorectal cancer cells (HCT116 cells) were incubated with the nanoparticles for 6 hours, washed with PBS, and collected in a 0.2 mL tube. The untreated cells were also used as a control. As shown in Figure 3, the tube containing the control cells was fairly dark, whereas the tube containing the cells treated with the Mn-HMAS nanoparticles became bright. These results indicated that the Mn-HMAS nanoparticles could be used as MRI contrast agents in vitro.

From Figure 4, we quantitatively calculated the loading of the drug DOX by measuring the change in absorbance before and after the adsorption of DOX in the mixture solution. The drug loading could reach 16.2% (*w*/*w*). To further test whether DOX release from Mn-HMAS-DOX could be triggered by pH, the drug release behaviours in PBS buffer at different pH values were evaluated. As shown in Figure 5, within the first 2 hours, in acidic PBS buffer solutions having a pH of 5.0 and 6.0, the release rate of the DOX was relatively faster than that in the neutral buffer solution at the pH level of 7.4. After 4 hours, the DOX release amount reached equilibrium. In a period of 12 hours, in the PBS buffer solutions, the drug release amounts were 38.1% for pH 7.4, 59.8% for pH 6.0, and 63.2% for pH 5.0.

To detect the toxic effects of Mn-HMAS nanoparticles on the growth of human colorectal cancer cell lines, we performed MTT assays on the colorectal cancer cell line HCT116 cells. The results confirmed that nanomaterials presented little cytotoxicity at low concentrations (Figure 6(a)), indicating the good biocompatibility of the blank carriers.

We next examined the therapy on HCT116 cells that were studied with stable concentrations of Mn-HMAS-DOX versus free DOX. Our results clearly demonstrated that Mn-HMAS-DOX nanoparticles exhibited a stronger inhibition efficiency than DOX (Figure 6(b)). At the same drug concentration (3.24 μg/mL), the inhibition rate of DOX was approximately 25%; however, the inhibition rate of Mn-HMAS-DOX nanoparticles was significantly increased to 52%. These results suggested that Mn-HMAS-DOX nanoparticles, loaded with DOX, may have a better ability to stimulate apoptosis. In addition, our study showed that Mn-HMAS-DOX nanoparticles stimulated morphological changes in HCT116 cells (Figure 7).

4. Conclusion

In conclusion, we first demonstrated that the Mn-HMAS nanoparticles could be used as *both an MRI contrast agent and a drug carrier*. The Mn-HMAS nanoparticles possessed good stability, noncytotoxicity, high drug-loading capacity, and high MR imaging performance. Moreover, our results also confirmed that Mn-HMAS-DOX nanoparticles present a better tumour cell inhibition effect than DOX. These features could make this nanosystem a promising material for the treatment of deeply located cancers.

Data Availability

The data used to support the findings of this study are included within the article.

Conflicts of Interest

The authors declare that they have no conflicts of interest.

Authors' Contributions

Yue Lu and Shirui Zhao contributed equally to this work.

Acknowledgments

This study was financially supported by the National Natural Science Foundation of China (grant no. 81572243) and the Scientific Research Funds Project of Liaoning Education Department (LJC2019ST02).

Supplementary Materials

Figure S1: size distribution of the [Mn]-HMAS nanoparticles in aqueous solution. Figure S2: zeta potential of the [Mn]-HMAS nanoparticles in aqueous solution. *(Supplementary Materials)*

References

[1] L. A. Torre, F. Bray, R. L. Siegel, J. Ferlay, J. Lortet-Tieulent, and A. Jemal, "Global cancer statistics, 2012," *CA: a Cancer Journal for Clinicians*, vol. 65, no. 2, pp. 87–108, 2015.

[2] A. Tenesa and M. G. Dunlop, "New insights into the aetiology of colorectal cancer from genome-wide association studies," *Nature Reviews Genetics*, vol. 10, no. 6, pp. 353–358, 2009.

[3] M. Arnold, M. S. Sierra, M. Laversanne, I. Soerjomataram, A. Jemal, and F. Bray, "Global patterns and trends in colorectal cancer incidence and mortality," *Gut*, vol. 66, no. 4, pp. 683–691, 2017.

[4] Y. Zhou, S. Li, Y. P. Hu et al., "Blockade of EGFR and ErbB2 by the novel dual EGFR and ErbB2 tyrosine kinase inhibitor GW572016 sensitizes human colon carcinoma GEO cells to apoptosis," *Cancer Research*, vol. 66, no. 1, pp. 404–411, 2006.

[5] W. De Roock, V. De Vriendt, N. Normanno, F. Ciardiello, and S. Tejpar, "*KRAS* , *BRAF* , *PIK3CA* , and *PTEN* mutations: implications for targeted therapies in metastatic colorectal cancer," *The Lancet Oncology*, vol. 12, no. 6, pp. 594–603, 2011.

[6] J. Terzic, S. Grivennikov, E. Karin, and M. Karin, "Inflammation and colon cancer," *Gastroenterology*, vol. 138, no. 6, pp. 2101–2114.e5, 2010.

[7] J. E. Lee, N. Lee, T. Kim, J. Kim, and T. Hyeon, "Multifunctional mesoporous silica nanocomposite nanoparticles for theranostic applications," *Accounts of Chemical Research*, vol. 44, no. 10, pp. 893–902, 2011.

[8] F.-P. Chang, Y. Hung, J.-H. Chang, C.-H. Lin, and C.-Y. Mou, "Enzyme encapsulated hollow silica nanospheres for intracellular biocatalysis," *ACS Applied Materials & Interfaces*, vol. 6, no. 9, pp. 6883–6890, 2014.

[9] S. Yang, D. Chen, N. Li et al., "Hollow mesoporous silica nanocarriers with multifunctional capping agents for in vivo cancer imaging and therapy," *Small*, vol. 12, no. 3, pp. 360–370, 2016.

[10] M. Wu, Q. Meng, Y. Chen et al., "Large Pore-Sized Hollow Mesoporous Organosilica for Redox-Responsive Gene Delivery and Synergistic Cancer Chemotherapy," *Advanced Materials*, vol. 28, no. 10, pp. 1963–1969, 2016.

[11] Y. Li, N. Li, W. Pan, Z. Yu, L. Yang, and B. Tang, "Hollow mesoporous silica nanoparticles with tunable structures for controlled drug delivery," *ACS Applied Materials & Interfaces*, vol. 9, no. 3, pp. 2123–2129, 2017.

[12] Z. Zou, S. Li, D. He et al., "A versatile stimulus-responsive metal–organic framework for size/morphology tunable hollow mesoporous silica and pH-triggered drug delivery," *Journal of Materials Chemistry B*, vol. 5, no. 11, pp. 2126–2132, 2017.

[13] S. P. Hadipour Moghaddam, M. Yazdimamaghani, and H. Ghandehari, "Glutathione-sensitive hollow mesoporous silica nanoparticles for controlled drug delivery," *Journal of Controlled Release*, vol. 282, pp. 62–75, 2018.

[14] T. Li, T. Geng, A. Md, P. Banerjee, and B. Wang, "Novel scheme for rapid synthesis of hollow mesoporous silica nanoparticles (HMSNs) and their application as an efficient delivery carrier for oral bioavailability improvement of poorly water-soluble BCS type II drugs," *Colloids and Surfaces B: Biointerfaces*, vol. 176, pp. 185–193, 2019.

[15] L. Jin, Q.-J. Huang, H.-Y. Zeng, J.-Z. Du, S. Xu, and C.-R. Chen, "Hydrotalcite-gated hollow mesoporous silica delivery system for controlled drug release," *Microporous and Mesoporous Materials*, vol. 274, pp. 304–312, 2019.

[16] D. Kim, K. Shin, S. G. Kwon, and T. Hyeon, "Synthesis and biomedical applications of multifunctional nanoparticles," *Advanced Materials*, vol. 30, no. 49, article 1802309, 2018.

[17] V. Dahanayake, C. Pornrungroj, M. Pablico-Lansigan et al., "Paramagnetic clusters of Mn_3 $(O_2CCH_3)_6(Bpy)_2$ in polyacrylamide nanobeads as a new design approach to a T_1–T_2 multimodal magnetic resonance imaging contrast agent," *ACS Applied Materials & Interfaces*, vol. 11, pp. 18153–18164, 2019.

[18] Y. Chen, H. Chen, Y. Sun et al., "Multifunctional mesoporous composite nanocapsules for highly efficient MRI-guided high-intensity focused ultrasound cancer surgery," *Angewandte Chemie International Edition*, vol. 50, no. 52, pp. 12505–12509, 2011.

[19] D. Kim, J. Kim, Y. I. Park, N. Lee, and T. Hyeon, "Recent development of inorganic nanoparticles for biomedical imaging," *ACS Central Science*, vol. 4, no. 3, pp. 324–336, 2018.

[20] Q. Liu, M. Xu, T. Yang, B. Tian, X. Zhang, and F. Li, "Highly photostable near-IR-excitation upconversion nanocapsules based on triplet–triplet annihilation for in vivo bioimaging application," *ACS Applied Materials & Interfaces*, vol. 10, no. 12, pp. 9883–9888, 2018.

[21] H. Cabral, N. Nishiyama, and K. Kataoka, "Supramolecular nanodevices: from design validation to theranostic nanomedicine," *Accounts of Chemical Research*, vol. 44, no. 10, pp. 999–1008, 2011.

[22] C. Sun, H. Zhang, S. Li et al., "Polymeric nanomedicine with "Lego" surface allowing modular functionalization and drug encapsulation," *ACS Applied Materials & Interfaces*, vol. 10, no. 30, pp. 25090–25098, 2018.

[23] D. Pan, A. H. Schmieder, S. A. Wickline, and G. M. Lanza, "Manganese-based MRI contrast agents: past, present, and future," *Tetrahedron*, vol. 67, no. 44, pp. 8431–8444, 2011.

[24] X. Fang, Z. Liu, M.-F. Hsieh et al., "Hollow mesoporous aluminosilica spheres with perpendicular pore channels as catalytic nanoreactors," *ACS Nano*, vol. 6, no. 5, pp. 4434–4444, 2012.

[25] W. Fang, L. Ma, J. Zheng, and C. Chen, "Fabrication of silver-loaded hollow mesoporous aluminosilica nanoparticles and their antibacterial activity," *Journal of Materials Science*, vol. 49, no. 9, pp. 3407–3413, 2014.